

## Original Article

# New approach for predictive measurement of knee cartilage defects with three-dimensional printing based on CT-arthrography: A feasibility study



R. Michalik<sup>a,\*</sup>, S. Schradling<sup>b</sup>, T. Dirrachs<sup>b</sup>, A. Prescher<sup>c</sup>, C.K. Kuhl<sup>b</sup>, M. Tingart<sup>a</sup>, B. Rath<sup>a</sup>

<sup>a</sup> Department of Orthopaedic Surgery, University Hospital RWTH Aachen, Aachen, Germany

<sup>b</sup> Department of Diagnostic and Interventional Radiology, University Hospital RWTH Aachen, Aachen, Germany

<sup>c</sup> Institute of Molecular and Cellular Anatomy, University RWTH Aachen, Aachen, Germany

## ARTICLE INFO

## Article history:

Received 21 August 2016

Accepted 13 October 2016

Available online 31 October 2016

## Keywords:

3D-Printing

Articular knee cartilage

CT-Arthrography

Cartilage defect

Preoperative planning

## ABSTRACT

**Purpose:** The aim was to prove the possibility of creating an exact module of knee cartilage defects using 3D printing.

**Methods:** Defects were created in cadaver knees. CT-arthrography and 3-Tesla MRI were performed. Based on CTA images a model of the cartilage was created using 3D printing. Defect-sizes in the imaging modalities were compared.

**Results:** Estimated lesion area in 3D model differed approximately 5% comparing to the defect sizes in knees. MRI underestimated the defect on average of 12%, whereas the CTA overestimated the defect about 3%.

**Conclusions:** We proved the feasibility of creating an accurate module of knee cartilage.

© 2016 Prof. PK Surendran Memorial Education Foundation. Published by Elsevier, a division of RELX India, Pvt. Ltd. All rights reserved.

## 1. Introduction

Cartilaginous lesions are up to date an increasing problem in knee joint surgery.<sup>1–5</sup> These damages of the knee cartilage are caused by degenerative changes or trauma of the joint. Due to the demographic trend in western population, but also the increase of competitive and recreational sports, the number of focal cartilaginous injuries is on the rise among young and old population.<sup>1–10</sup> Defects of knee cartilage are not only causing chronic pain, decreased function and degeneration, they also lead to early-onset osteoarthritis of the knee, which is one of the diseases with the greatest impact on the economy and patients quality of life in western civilisation.<sup>1,11,12</sup> Present common treatment strategies depending on size and stage are bone marrow stimulation (e.g. microfracturing), autologous repair (osteochondral transplantation) and matrix associated techniques (e.g. matrix-induced chondrogenesis, autologous chondrocyte transplantation).<sup>1,10</sup> Marrow stimulation techniques like microfracturing were optimized by combination of the fixation of a biological scaffold to

cover the blood clot and permitting ingrowing mesenchyme stem cells to remain and differentiate into chondrogenetic cells.<sup>1,6–10</sup>

Diagnostic investigations and therapies of these pathologies improved within the last decade. However, the morphologic analysis of these defects is crucial for an adequate therapy strategy.<sup>1,11,12</sup> The size and extension of the cartilage lesion is one of the major determining factors when deciding what type of therapy procedure should be performed.<sup>5</sup> In preoperative diagnostics, the magnetic resonance imaging (MRI) nowadays is used as a “gold standard”. MRI is widely used for detecting internal derangements of the knee,<sup>13</sup> and is indicated in patients with signs and symptoms consistent with intra-articular pathology.<sup>5</sup> It is a non-invasive procedure, and has a low risk of complications. Nonetheless it was demonstrated, that size of cartilage defects is underestimated by preoperative MRI, which affect treatment strategies.<sup>14,15</sup> Therefore, improvements of imaging techniques are necessary and are in progress.

Compared to standard MRI with 3 Tesla field strength and 3 mm slice thickness, computed tomography arthrography (CTA) may have the potential to improve the visualization of cartilage lesions.<sup>16–18</sup> It benefits from the intra-articular injection of contrast fluid, and CTA has the advantage of a high spatial resolution as well as a high contrast between the hypodense cartilage and hyperdense surrounding bone and contrast fluid.<sup>16</sup>

\* Corresponding author at: Department of Orthopaedic Surgery, Aachen University Hospital, Pauwelsstraße 30, 52074 Aachen, Germany.

E-mail address: [rmichalik@ukaachen.de](mailto:rmichalik@ukaachen.de) (R. Michalik).

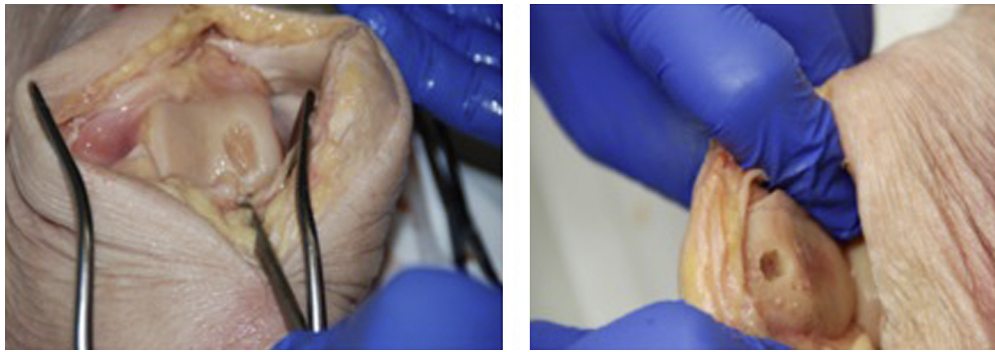


**Fig. 1.** Photographs demonstrating a typical cartilage defect of the femur condyle and the patella after debridement.

CTA has proven to be valuable diagnostic tools for the evaluation of internal derangement of e.g., the shoulder, particularly in the preoperative setting.<sup>16</sup>

With the rapidly advancing technique of three-dimensional printing (3D printing) a new technology is about to revolutionize medicine. 3D printing is a methodology using 3D CAD (computer-aided design) datasets for producing 3D physical model.<sup>19</sup> Also known as rapid prototyping, this technology is not only changing manufacturing industry, it also is being explored in many sections of medicine.<sup>20</sup> In many surgical fields this new technology was already used to create 3D objects of patients anatomy.<sup>19–22</sup> Some health care sectors are already experiencing the impact of 3D printing: dentistry and orthodontics are two examples.<sup>23</sup> More than 19,000 metal copings used to create crowns and bridges are up to date manufactured on 3D printing equipment.<sup>23</sup>

The principle of rapid prototyping is to use 3D computer models for the reconstruction of a 3D physical model by the addition of material layers.<sup>19</sup> Rapid prototyping has recently been introduced into the surgical area as a tool for better understanding of complex underlying anomaly.<sup>19</sup> These 3D models can improve and facilitate the diagnostic quality, were used for surgical planning, visualize complex anatomy and pathologies better and teach trainees in an unprecedented way.<sup>24</sup> Especially in orthopedic surgery 3D printing demonstrated a significant improvement in diagnosis and treatment due to better 3D appreciation of pathological structure, increased accuracy and possibility of preoperative planning.<sup>25</sup> In case of using prototype models, they can help to foresee intra-operative complications, and could also be used for implant planning and designing. The potential of the rapid prototyping technique lies within the possibility of e.g. customized cut blocks,<sup>26</sup> patient specific prostheses<sup>19</sup> and patient specific customized scaffolds for cartilage repair, respectively. Particularly the imaging of hyaline cartilage tissue and its defects have never been assessable in a haptic way regarding preoperative planning.

The purpose of this pilot study was to compare the diagnostic performance of standard CTA and standard MRI in assessing the cartilage of the knee and the feasibility of creating a accurate and vivid 3D model of knee cartilage by prospectively acquiring examinations with the three techniques in the same series of patients, with real defect measurement taken as a reference.

## 2. Materials and methods

We initiate a pilot study on three fresh-frozen human knees from two male donors mean age 88 years. The included objects were completely intact with no former pathologies. All organ donors gave written consent for anonymized use of their organs before death. Exclusion criteria for donated knee joints were history of knee trauma, osteosynthetic material, visible menisci or ligament pathologies and visible degeneration or damage of the cartilage tissue of the knee.

### 2.1. Cadaver specimen preparation

An arthrotomy was performed by an experienced orthopedic surgeon. Then a full thickness cartilage defect was placed in the trochlea region and the retropatellar area using a curette. Defects were created in different sizes measuring between 37 and 154 mm<sup>2</sup> (average sizing 91 mm<sup>2</sup>). Detailed pictures were taken of every lesion (Fig. 1). The capsule, the subcutaneous fat tissue and the skin then were closed surgically by an experienced surgeon. Subsequently all imaging procedures were performed by a radiological specialist.

### 2.2. MRI-imaging protocol

Each knee underwent a three tesla (3 T) MRI (Achieva 3 T, Philips Medical Systems, Eindhoven, The Netherlands). A dedicated 8-channel phased-array knee-coil was used and knees were examined in 30° angled stance. Knees were imaged in the axial, sagittal and coronal plane. The following sequences and parameters were performed:

- (1) T1-weighted turbo spin echo (TSE) sequences in axial, sagittal and coronal plane, recall acquisition in the steady state, flip angle 90°, repetition time 670 ms, echo time 15 ms, field of view 160 mm, slice thickness 3.0 mm, interslice gap 0.3 mm, 30 partitions, 320 × 320 matrix, two excitations, acquisition time 10 min 37 s.
- (2) Proton-density weighted (PDW) sequences in axial, sagittal and coronal plane, recall acquisition in the steady state, flip angle 90°, repetition time 3630 ms, echo time 15 ms, field of view 160 mm, slice thickness 3.0 mm, interslice gap 0.3 mm, 30 partitions, 320 × 320 matrix, one excitation, acquisition time 11 min 20 s.

### 2.3. CTA-imaging protocol

Every knee underwent an intraarticular contrast-enhanced 64-Multiple detector computed tomography (MDCT) (DEFITION 64; Siemens Healthcare, Forchheim, Germany). Knees were examined in relaxed state, fixed on a gel cushion. Intra-articular injection was performed anterolaterally with a 21 gauge needle. A 10 ml X-ray positive, low-osmolar iodine contrast medium (active ingredient: Iopamide/Solutrast 370, Bracco Imaging, Germany) was applied by an orthopedic specialist after dilution with saline solution (NaCl) (8 ml Solutrast/12 ml NaCl). The following imaging parameters were used: 120 kV, effective tube current-time product 92 mA, slice thickness 0.7 mm, rotation time 500 ms, pitch 0.9, and collimation 64 mm × 1.0 mm. The field-of-view was adapted to the individual subjects' physique, and a medium smooth convolution kernel (B30f) as well as a hard bone-window kernel

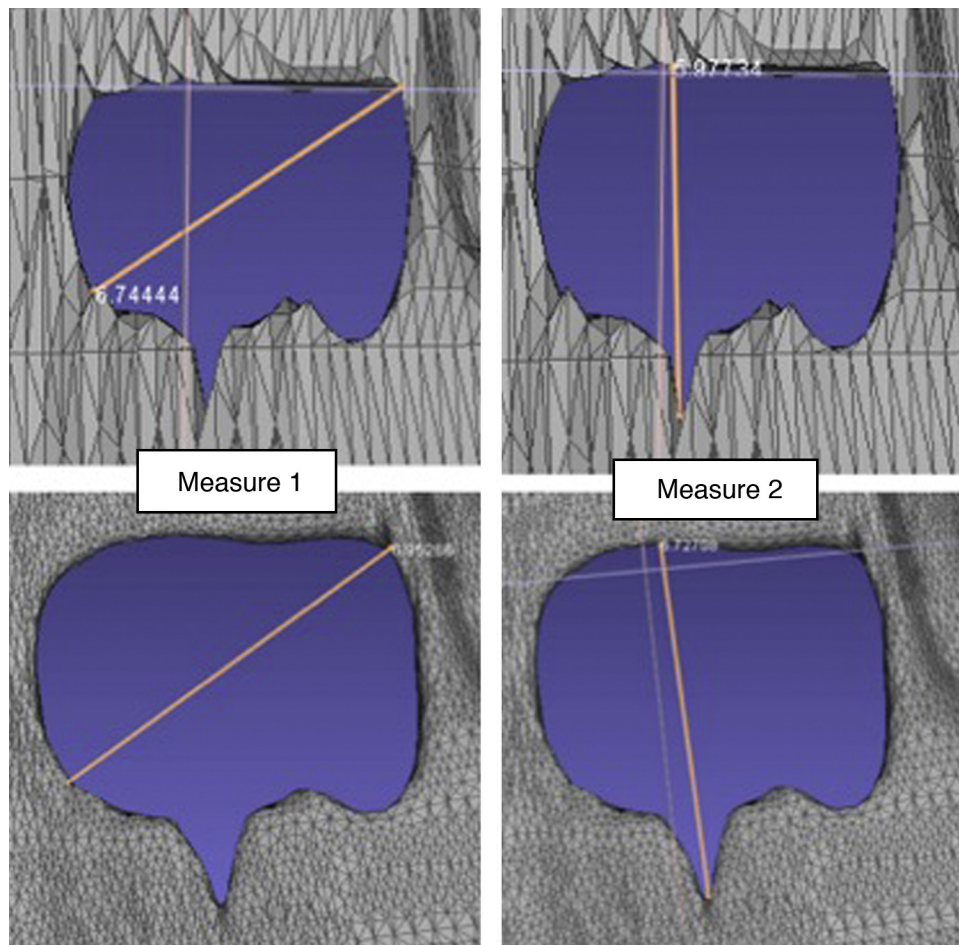


**Fig. 2.** The upper pictures show unfiltered femoral cartilage defect zone (measuring 6.74 mm, 5.98 mm). The filter criteria and settings were chosen to obtain real defect size but optimizing the surface structure for better printing results. The pictures below show the defect reconstruction after surface smoothing and creating an uniformly surface quality (measuring 6.95, 6.73 mm).

(B60f) were chosen for image reconstruction. Images were analyzed computer-aided with dedicated software (SyngoVia, Siemens, Forchheim, Germany).

#### 2.4. Image- and data-processing

The CT and MRI scans were available in widely recognized DICOM (Digital Imaging and Communications in Medicine) files.

For Segmentation we used the ITK-SNAP (v. 3.4 beta) software, a decent program for contour segmentation. It implements two well established 3D active contour segmentation methods: Geodesic Active Contours and Region Competition.<sup>27</sup> The segmentation was done semiautomatic by an experienced engineer.

The Data was transferred into standard tessellation language (STL) files. In a first step MeshLab (v.1.3.2\_64bit) and its filters were used to correct defects or surface errors in the STL file. The data was imported directly from ITK-SNAP software.

The following filters were used to process data:

- filters/cleaning and repairing/remove duplicated vertex
- filters/cleaning and repairing/remove unreferenced vertex
- filters/remeshing, simplification and reconstruction/subdivision surfaces: butterfly subdivision (default settings, edge threshold 0.33 world unit): to get a better surface quality.
- filters/smoothing, fairing, deformation/Laplacian smooth: default – settings are used. No cotangent weighting as this is creating surface inaccuracies.

- filters/cleaning and repairing/merge close vertices (abs merging distance 0.1 world unit)

The filter-settings were chosen especially regarding the high accuracy and exact reconstruction of the cartilage volume and defect size (Fig. 2).

#### 2.5. Three dimensional printing

In a second step, before final 3D printing, a stl-mesh processing (Fig. 3) was performed to ensure a trouble-free and accurate 3D model for printing.

For printing the STL data we used an Ultimaker 2.0 (Ultimaker, Netherlands). The printer works with Fused Filament Fabrication (FFF) print technology and melts plastic and deposits it on a glass plate in an additive process. Speed range from 30 to 300 mm per second, enabling fast prints or slow, high-quality prints. Resolution is about 0.02 mm per print layer. It is also possible to adjust settings during the printing process so that, if a problem is noticed, it can be corrected without restarting the print. The Ultimaker 2 supports the two most popular printing filaments: Acrylnitril-Butadien-Styrol-Copolymerisat (ABS) and polylactic acid (PLA).

In this study we used a resolution of 0.1 mm slice thickness printing the 3D models of the knee cartilage and their defect. The shape accuracy for 3D printing was the same than CT accuracy. The models were created from ABS – thermoplastic filament, as this material is impact resistant, very hard, whilst retaining good

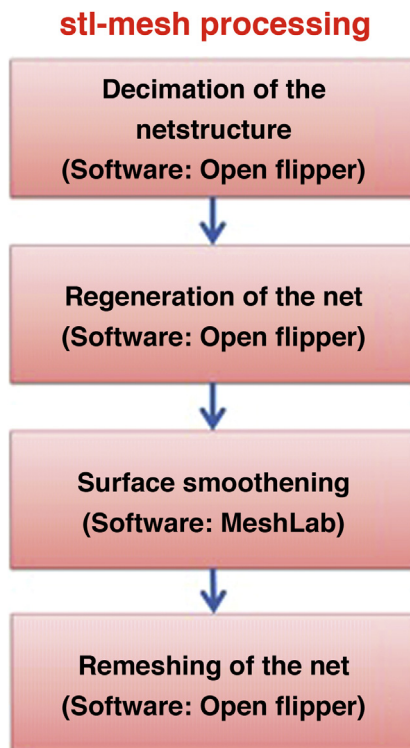


**Fig. 3.** Workflow of the stl-mesh processing with MeshLab (v.1.3.2\_64bit) and Open flipper (v. 2.1, <http://www.openflipper.org/>).

flexibility. We created models of the patellar and femoral cartilage layer containing the full sized defect. Also it was feasible of printing a 3D module of the defect zone.

#### 2.6. Statistics

Statistical analysis was performed with use of IBM SPSS Statistics software (Version 22.0.0.0) and Microsoft Excel (for Mac 2011, v. 14.0.0).

Differences between the imaging modalities were considered to be statistically significant if  $p < 0.05$  (*t*-test for independent samples).

To assess and display agreement between two methods of measurement Bland–Altman-Plot was used. Mean and difference

between measured defect sizes were displayed. Lines of agreement were set mean – and +1.96 standard deviation. Between these lines a third line represents the mean of the difference. As more than 95% of the differences lie in between the lines of agreement, the two compared methods of clinical measurement were considered to show a good agreement.

### 3. Results

#### 3.1. MRI imaging

MRI scanning time for each knee joint amounted to approximately 22 min. The cartilage tissue and the defect zone were accessed in axial, coronal and sagittal orientation. The MRI had no limitations in accessing all parts of the knee joint and its covering cartilage tissue. The defect zones localized at the medial femoral condyle and the posterior patella were definable as sharp margined hyperintense areas in the PDW sequence (Fig. 4).

#### 3.2. CTA imaging

CTA scanning time accounted approximately 5 s. The knee joint and its structures were accessed in three orientations (axial, coronal and sagittal). The hyaline cartilage is seen as a structure of low attenuation. It is delimited by the subchondral bone on the one and the hyperintense contrast agent on the other side. The penetration of contrast agent in the cartilage tissue definitely indicates the defect zone. Detection of both patellofemoral and tibiofemoral joint lesions was possible in all cases. As the contrast agent rinsed the defect zones those were excellent accessible as well defined hyperintense areas. The combination of high spatial resolution and high-attenuation difference between the cartilage tissue and the contrast material filling the lesion were an advantage compared to the MRI (Fig. 5).

#### 3.3. Segmentation and 3D printing

Segmentation of DICOM images proved to be feasible in all cases. The CTA images with its high resolution and the so acquired 3D reconstruction after segmentation, has a smooth surface structure which is great for further processing and 3D printing of a vivid and realistic model (Fig. 6b). The segmentation of 3D images based on MRI was also feasible. Due to slice thickness of 3 mm and the 0.3 mm intersection gap the digital reconstruction shows a stepped and layered surface texture (Fig. 6c).

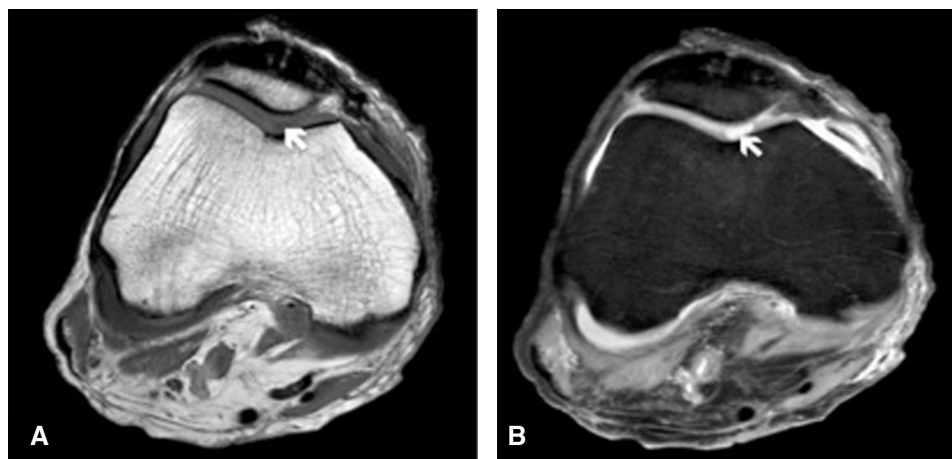


**Fig. 4.** (a) Axial reformatted image obtained after MRI T1-weighted turbo spin echo sequences. Cartilage defect of the femur (white arrow) can only be discovered with difficulty as a hypointense area. (b) Axial reformatted image obtained after Proton-density weighted (PDW) sequence showing the defect of cartilage tissue as a sharp margined hyperintense area of the femur (white arrow).

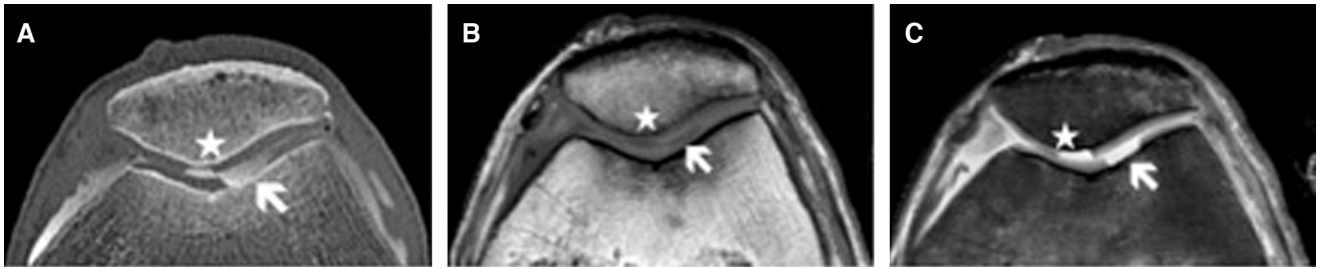


**Fig. 5.** (a) Axial reformatted image obtained after spiral CTA of the knee. Contrast agent filling a full sized cartilage defect of the femur (white arrow) and the patellar (white star). MRI images in axial plane depict cartilage defects of the femur (white arrow) and retro patellar region (white star). In T1-weighted turbo spin echo sequence the defect zone is displayed as a hypointense area (b). Proton-density weighted (PDW) sequence shows the defect of cartilage tissue as a well defined hyperintense area (c).

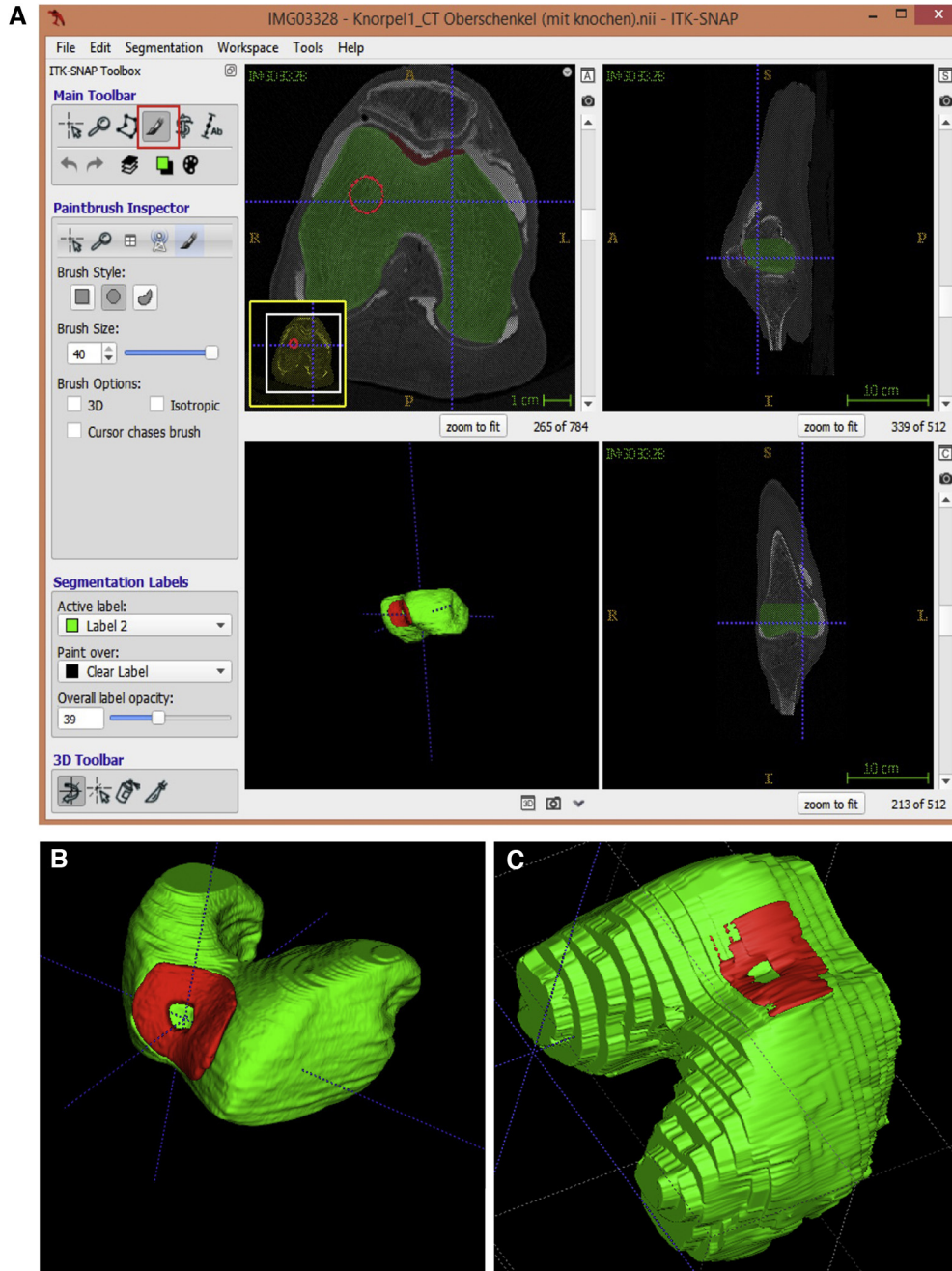


**Fig. 6.** (a) Segmentation process of the distal femur based on CTA image. Process is working semiautomatic. Cartilage tissue in the trochlea (red) contains a full sized defect zone. (b) 3D image based on segmentation of CTA data shows a smooth and vivid structure. (c) The segmented 3D image based on 3 T MRI has a stepped and pixelated surface structure.

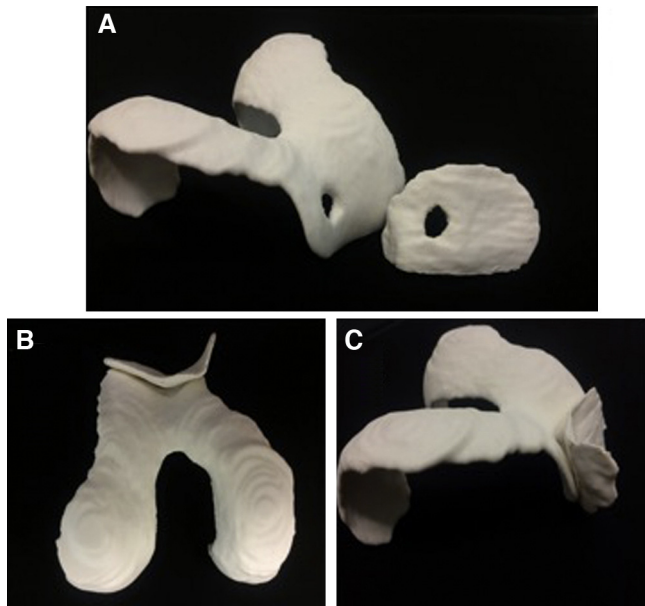


**Fig. 7.** ABS model of the articular retropatellar and femoral cartilage. Both models containing a full-size cartilage defect. The different captures show the well defined defect zones (a) and the great fit of the articulating components from bottom (b) and side view (c).

Printing of the ABS module of the cartilage-cover of the knee joint accounted approximately 5 h. Printed were the retropatellar cartilage and the femoral cartilage cover out of solid and desinfectable abs plastic (Fig. 7).

After full data acquisition the approximate defect area was calculated, measured length by width. Measured defect size in the specimen, CTA, MRI and the defect size in the printed 3D model were compared. Then the results were statistically analyzed. Ground truth was defect size in the specimen.

Differences between measured size of cartilage defects in specimen, and CTA were not statistically significant ( $p = 0.09$ ).

The Bland–Altman – plot shows good agreement between measurements as all of the differences lie between the lines of agreement (Fig. 8a).

Differences between measured size of cartilage defects in specimen and 3D printing were not statistically significant ( $p = 0.071$ ). The Bland–Altman – Plot shows good agreement with all data in between the lines of agreement (Fig. 8b).

Differences between measured size of cartilage defects in specimen and MRI were statistically significant ( $p = 0.013$ ) as well as the differences in MRI and CTA ( $p = 0.013$ ), and also MRI and 3D module ( $p = 0.011$ ).

Differences between measured size of cartilage defects in CTA and 3D module were not statistically significant ( $p = 0.733$ ). The Bland–Altman – Plot shows good agreement (Fig. 8c).

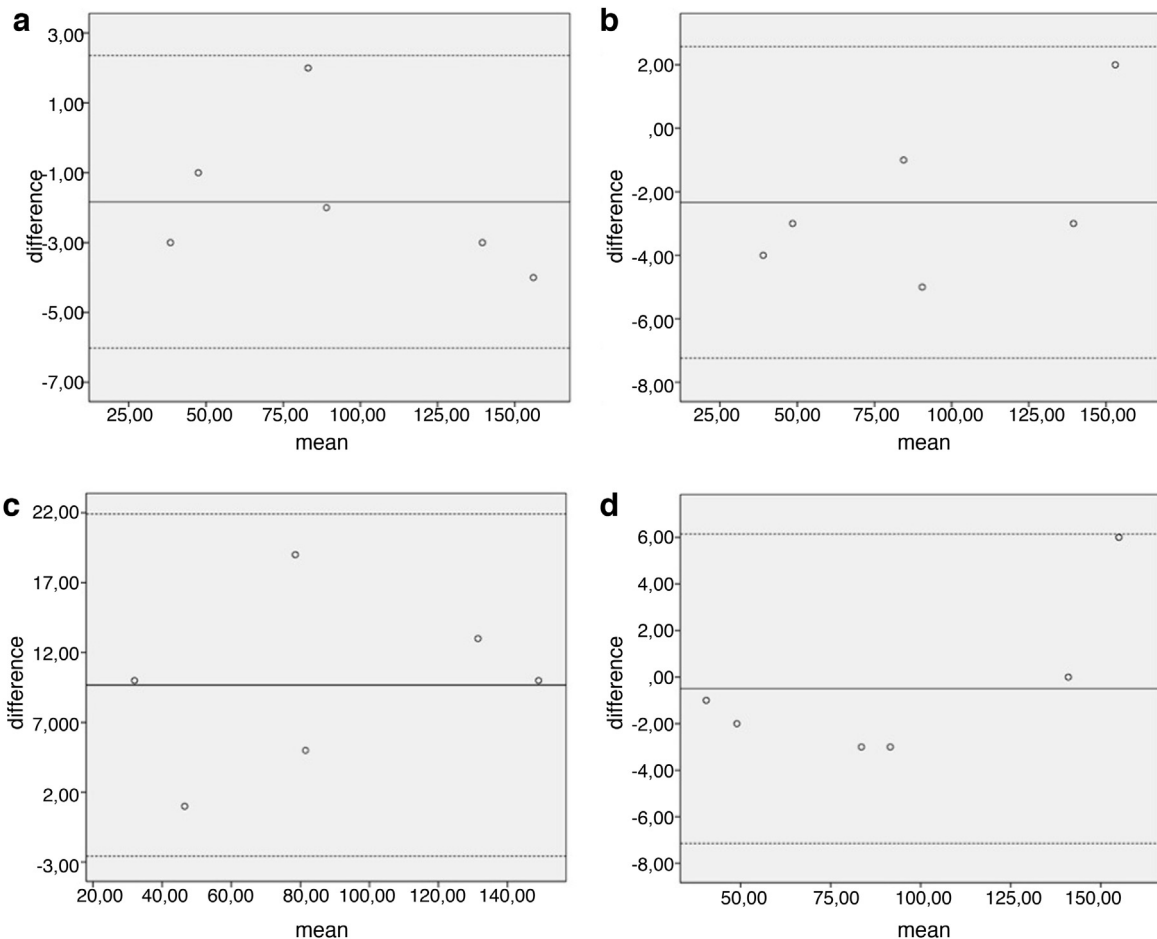


**Fig. 8.** (a–d) Bland– Altman – plot comparing the methods of imaging concerning cartilage defects (measured in mm<sup>2</sup>). The graph displays a scatter diagram of the differences plotted against the mean of the two methods measurements of defect size in two different imaging modalities. (a) Comparing measurement in specimen and CTA. Limits of agreement were set 2.3 and –6. Mean was calculated –1.833. (b) Measurement in Specimen and 3D model were compared. Limits of agreement were set 2.57 and –7.23. Mean was calculated –2.33. (c) Measurement in Specimen was compared to 3 T MRI. The Limits of agreement were set 6.14 and –7.14. Mean was calculated –0.5. (d) Comparing measurement in CTA to 3D model. Limits of agreement were set –2.59 and 21.91. Mean was calculated 9.66.

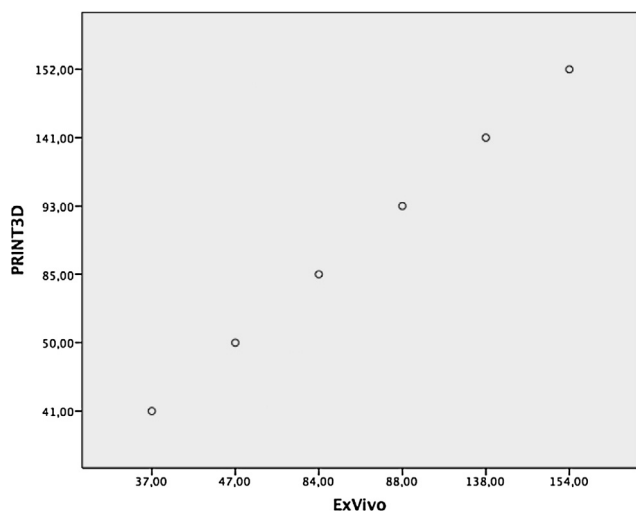


**Fig. 9.** Defect area (in mm<sup>2</sup>) measured ExVivo in specimen displayed on coordinate axis (ExVivo) compared to defect area measured in printed 3D model displayed on axis of ordinates (PRINT3D) were compared. The 6 defects were displayed in ascending order.

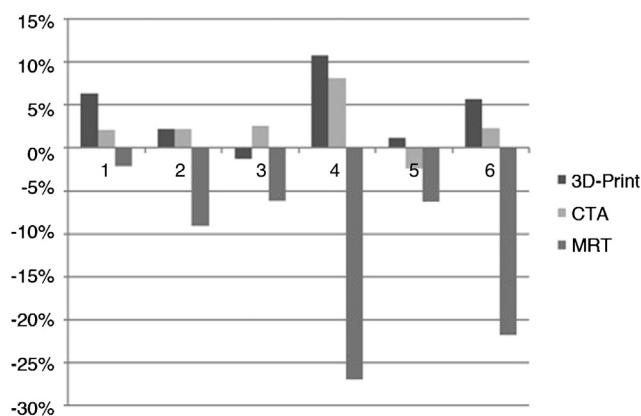


**Fig. 10.** Deviation of cartilage defect size based on different imaging modalities compared to defect size in specimen used as reference standard. 1–6 referring to the different lesions of the knee cartilage. Defects 1–3 localized in trochlea groove of the femur, 4–6 in the retropatellar cartilage.

Data analysis shows that measuring the size of cartilage defect based on MRI, the approx. defect size is underestimated in all 6 cases (Fig. 8d).

To calculate correlation between measured defect size in specimen (ExVivo) and 3D print the Pearson – correlation coefficient was used (Fig. 9). The size of defect areas measured shows a significant correlation ( $r = 1$ ).

Deviation of MRI from the measured cartilage defect size in specimen (specimen used as standard reference) shows a mean difference of  $\pm 12\%$  (Fig. 10).

Comparing defect size measured in CTA imaging and specimen, the data shows that CTA might slightly overestimate the size of the lesion. The mean difference in size is calculated  $\pm 3\%$ .

Through further image processing and 3D active contour segmentation using MeshLab the registered defect size differs  $\pm 3\%$  in mean from the CTA image and 5% from the specimen.

#### 4. Discussion

To the authors' knowledge this is the first study, which assessed the performance of 3D printing of cartilage lesions for the case of preoperative therapy planning.

The adequate diagnostics and treatment of chondral or osteochondral lesions of the articular cartilage is crucial to prevent the development of early onset osteoarthritis. Moreover, adequate imaging and measuring of defect size and shape are necessary to allow preoperative planning, treatment strategy, and surgical access.<sup>1,6,7,9,10</sup>

The MRI is the imaging modality of choice (“gold standard”) for the assessment of articular cartilage. However, it remains a pricy and time-consuming method that shows several limitations when used in a standard setup. It was demonstrated, that the size of cartilage defects is underestimated by preoperative MRI, which could affect treatment strategies.<sup>14</sup> In a study from Gomoll et al. the size of cartilage defects measured preoperatively by high-resolution MRI with surgical measurements were compared. It was shown that the majority of defects was underestimated by MRI over 60% in size.<sup>15</sup> Our results show an underestimation of cartilage defect zones of 12% mean from the original defect. One of the reasons might be the slice thickness used by the standard MRI examination in the diagnostics of cartilage lesions. Standard is a slice thickness of 3 mm, which may lead to measurement inaccuracy. Also the images are performed with an interslice gap of 0.3 mm.

Other limitations of MRI imaging in clinical practice are Patients with claustrophobia or ferromagnetic implants like an implanted defibrillator or deep brain stimulator.<sup>28,29</sup> In our study we used as an alternative to MRI the CTA based images for the segmentation,

adding contrast agent to image defect zones of the cartilage tissue. Previous studies already showed that CTA compared to MRI is a valuable method for depiction of cartilage lesions of the knee with high sensitivity and specificity.<sup>16,28</sup> Studies from Vande Berg et al. and Gagliardi et al. even showed that CTA can be superior in the detection of chondral lesions of the knee joint compared to standard MRI.<sup>17,18</sup>

Using a section thickness of 0.7 mm and contrast agent a realistic and accurate assessment of the cartilage and defect zone was possible. As the results show, CTA could enable a more accurate depiction and measurement of defect-size. Mean difference of defect size was 3% compared to specimen. The so obtained accuracy in imaging was mandatory for further processing and the accurate creation of the 3D model.

Moreover, examination of each knee with CTA was approximately more than 20 min shorter. Also the limitations of the MRI scan like implanted ferromagnetic material or electronic devices and claustrophobia are no barrier for CTA. On the other hand the use of CT scan due to ionizing radiation is limited in pregnancy and its use on children.<sup>30,31</sup> Also the slight invasiveness of CTA imaging injecting contrast agent is one of the disadvantages.

Still none of the standard imaging modalities provides a three dimensional, haptic and vivid module of the region of interest, which makes shape and size of the pathology graspable for the surgeon to ease pre- and intraoperative planning.

The clinical use of three-dimensional printing or so-called rapid prototyping is still in an early phase but previous studies with three-dimensional printers and their products in different surgical cases and disciplines recognized their potential in patient education, surgical planning and clinical training.<sup>19,20,22</sup>

In this context, the main aim of our study was to prove feasibility of creating a three-dimensional model of articular knee cartilage and a containing defect zone. Furthermore, we determined a setup and developed a process-chain for optimal results, respectively.

The results show that CTA based 3D printouts of cartilage defects, as they were processed as described, have a high accuracy with only 5% deviation of the specimen (Fig. 8). Defect size has been slightly overestimated in 5 of 6 cases. The ABS model represents the defect zone in mean more accurate than the MRI

and has a mean deviation of 5% from the specimen what is within clinical exceptions. As the CTA based three-dimensional printout shows not only high accuracy, but also surpasses the “gold standard” MRI in agreement compared to specimen, it is certainly a gain in preoperative imaging.

For the orthopedic and trauma surgeon the new approach also simplifies preoperative planning and choice of the suited procedure and access.

Regarding the treatment of cartilage defects sizing <1.5 cm<sup>2</sup> with an AMIC surgery the visualization of the knee cartilage and the defect (in bird perspective) is only intraoperative possible. The surgery begins with an arthroscopy to verify the size and location of the defect. Then the arthrotomy is performed for assessment of the defect, debridement, microfracture and then to customize the matrix for implantation.

Using 3D printing for creating a model of the defect zone the preparation of the scaffold is possible sparing the arthrotomy. By using the 3D model planning and preparation of the scaffold can be done preoperatively. After arthroscopic debridement and microfracturing the customized scaffold can be inserted arthroscopically. The model is made out of robust ABS plastic than can be completely sterilized and be taken for intraoperative use in the operating room. The use of CTA based three-dimensional printouts of intraarticular knee cartilage is therefore not only a new approach in preoperative diagnostics. It opens up a new possibility for performing cartilage repair techniques in a complete arthroscopic technique. The scaffold can be customized previous to the operation and save not only resources but also reduce operation time and trauma. The 3D print allows us to plan surgery on an exact and vivid model.

#### 4.1. Limitations

Our study had several limitations due to the small number of specimen and the use of cadaver knees. The lack of active mobilization of the joint may affect distribution of contrast agent before CTA and lack of intraarticular fluid in cadaver knees interfere with MR imaging.<sup>18</sup> The use of a small number of cadaver knees with lack of osteoarthritic changes may affect the imaging and results.

## 5. Conclusions

Recent work already demonstrated, that other disciplines in medicine already integrated the challenging workflow of rapid prototyping and its benefits successfully in their clinical routine.<sup>19</sup> Our study, comparing various methods of 3D imaging techniques combined with 3D printing, confirmed that this approach including 3D printing can be reliably performed for morphological cartilage imaging of the knee and reconstruction of cartilage lesion, respectively. Further advantages like development of new surgical strategies like an arthroscopic approach will be part of further research. The goal is to minimize operation trauma and time, reduce possible complications as infection and also allow a better cosmetic result. In our study we showed the feasibility of creating an image based accurate 3D model of knee cartilage and its defects. Further studies with larger number of specimen and standardized defect size are in planning to prove the daily use of the 3D model and its reproducibility. Furthermore the feasibility of using the less invasive high resolution MRI as a 3D printing based imaging modality instead of CTA will be part of further research. The workflow will be integrated in the standard operating procedure of cartilage repair, proving the outlined benefits of the 3D print in knee surgery.

## Conflicts of interest

The authors have none to declare.

## Acknowledgments

The authors would like to thank Dr. Jörg Eschweiler for his assistance and Mrs. Britta Kremers for image acquisition and technical support.

## References

- Turkiewicz A, Petersson IF, Bjork J, et al. Current and future impact of osteoarthritis on health care: a population-based study with projections to year 2032. *Osteoarthr Cartil.* 2014;22(November (11)):1826–1832.
- Mithoefer K, Saris DBF, Farr J, et al. Guidelines for the design and conduct of clinical studies in knee articular cartilage repair: international cartilage repair society recommendations based on current scientific evidence and standards of clinical care. *Cartilage.* 2011;2(March (2)):100–121.
- Lee YHD, Suzer F, Thermann H. Autologous matrix-induced chondrogenesis in the knee: a review. *Cartilage.* 2014;5(June (3)):145–153.
- Hjelle K, Solheim E, Strand T, Muri R, Brittberg M. Articular cartilage defects in 1000 knee arthroscopies. *Arthroscopy.* 2002;18(September (7)):730–734.
- Mall NA, Harris JD, Cole BJ. Clinical evaluation and preoperative planning of articular cartilage lesions of the knee. *J Am Acad Orthop Surg.* 2015;23(October (10)):633–640.
- Buckwalter JA, Lohmander S. Operative treatment of osteoarthritis. Current practice and future development. *J Bone Joint Surg Am.* 1994;76(September (9)):1405–1418.
- Cole BJ, Pascual-Garrido C, Grumet RC. Surgical management of articular cartilage defects in the knee. *Instr Course Lect.* 2010;59:181–204.
- Braun S, Vogt S, Imhoff AB. Stage oriented surgical cartilage therapy. Current situation. *Orthopäde.* 2007;36(June (6)):589–599.
- Oeppen RS, Connolly SA, Bencardino JT, Jaramillo D. Acute injury of the articular cartilage and subchondral bone: a common but unrecognized lesion in the immature knee. *Am J Roentgenol.* 2004;182(January (1)):111–117.
- Upmeier H, Brüggjenjürgen B, Weiler A, Flamme C, Laprell H, Willich SN. Follow-up costs up to 5 years after conventional treatments in patients with cartilage lesions of the knee. *Knee Surg Sports Traumatol Arthrosc.* 2006;15(December (3)):249–257.
- Gelber AC, Hochberg MC, Mead LA, Wang NY, Wigley FM, Klag MJ. Joint injury in young adults and risk for subsequent knee and hip osteoarthritis. *Ann Intern Med.* 2000;133(September (5)):321–328.
- Felson DT. Clinical practice. Osteoarthritis of the knee. *N Engl J Med.* 2006;354(February (8)):841–848.
- Mattila VM, Weckstrom M, Leppanen V, Kiuru M, Pihlajamaki H. Sensitivity of MRI for articular cartilage lesions of the patellae. *Scand J Surg.* 2012;101(1):56–61.
- Campbell AB, Knopp MV, Kolovich GP, et al. Preoperative MRI underestimates articular cartilage defect size compared with findings at arthroscopic knee surgery. *Am J Sports Med.* 2013;41(March (3)):590–595.
- Gomoll AH, Yoshioka H, Watanabe A, Dunn JC, Minas T. Preoperative measurement of cartilage defects by MRI underestimates lesion size. *Cartilage.* 2011;2(October (4)):389–393.
- Omoumi P, Rubini A, Dubuc J-E, Vande Berg BC, Lecouvet FE. Diagnostic performance of CT-arthrography and 1.5 T MR-arthrography for the assessment of glenohumeral joint cartilage: a comparative study with arthroscopic correlation. *Eur Radiol.* 2014;25(November (4)):961–969.
- Gagliardi JA, Chung EM, Chandnani VP, et al. Detection and staging of chondromalacia patellae: relative efficacies of conventional MR imaging, MR arthrography, and CT arthrography. *Am J Roentgenol.* 1994;163(September (3)):629–636.
- Vande Berg BC, Lecouvet FE, Poilvache P, et al. Assessment of knee cartilage in cadavers with dual-detector spiral CT arthrography and MR imaging. *Radiology.* 2002;222(February (2)):430–436. Available from: <http://eutils.ncbi.nlm.nih.gov/entrez/eutils/elink.fcgi?dbfrom=pubmed&id=11818610&retmode=ref&cmd=prlinks>
- Rengier F, Mehndiratta A, Tengg-Kobligh von H, et al. 3D printing based on imaging data: review of medical applications. *Int J CARS.* 2010;5(May (4)):335–341.
- Marro A, Bandukwala T, Mak W. Three-dimensional printing and medical imaging. A review of the methods and applications. *Curr Prob Diagn Radiol.* 2016;45(January (1)):2–9.
- Mendez BM, Chiodo MV, Patel PA. Customized “In-Office” three-dimensional printing for virtual surgical planning in craniofacial surgery. *J Craniofac Surg.* 2015;26(July (5)):1584–1586.
- Waran V, Narayanan V, Karupiah R, et al. Injecting realism in surgical training – initial simulation experience with custom 3D models. *J Surg Educ.* 2014;71(2):193–197.
- Möller C, Durand C. *Biomedical 3-d Printing BCG Perspectives.* 2015, September;1–7.
- Costello JP, Olivieri LJ, Su L, et al. Incorporating three-dimensional printing into a simulation-based congenital heart disease and critical care training curriculum for resident physicians. *Congenit Heart Dis.* 2015;10(January (2)):185–190.
- Tam MD, Laycock SD, Bell D, Chojnowski A. 3-D printout of a DICOM file to aid surgical planning in a 6 year old patient with a large scapular osteochondroma complicating congenital diaphyseal acasia. *J Radiol Case Rep.* 2012;6(January (1)):31–37.

26. Radermacher K, Portheine F, Anton M, et al. Computer assisted orthopaedic surgery with image based individual templates. *Clin Orthop Relat Res*. 1998, September;354:28–38.
27. Yushkevich PA, Piven J, Hazlett HC, et al. User-guided 3D active contour segmentation of anatomical structures: significantly improved efficiency and reliability. *NeuroImage*. 2006;31(3):1116–1128.
28. De Filippo M, Bertellini A, Pogliacomi F, et al. Multidetector computed tomography arthrography of the knee: diagnostic accuracy and indications. *Eur J Radiol*. 2009;70(May (2)):342–351.
29. Melendez JC, McCrank E. Anxiety-related reactions associated with magnetic resonance imaging examinations. *J Am Med Assoc*. 1993;270(August (6)):745–747.
30. Lowe SA. Diagnostic radiography in pregnancy: risks and reality. *Aust N Z J Obstet Gynaecol*. 2004;44(June (3)):191–196.
31. Spycher BD, Lupatsch JE, Zwahlen M, et al. Background ionizing radiation and the risk of childhood cancer: a census-based nationwide cohort study. *Environ Health Perspect*. 2015;123(June (6)):622–628.